Supplementary Information

Microphysical Properties and Ice Crystal Habits of Low-Level Arctic Mixed-Phase Clouds from Four Airborne In Situ Campaigns over the Svalbard Seas

Aymeric Dziduch[1], Antoine Baudoux[1], Guillaume Mioche[1], Antoine Canzi[1], Benjamin Doiteau[1], Manuel Moser[2], Emma Järvinen[3], Étienne Vignon[4], Jean-Christophe Raut[5], Régis Dupuy[1], Christophe Gourbeyre[1], Jean-Luc Baray[1], Marie Monier[1], Frédéric Szczap[1], Guillaume Penide[6], Julien Delanoë[5], Odran Sourdeval[6], Alfons Schwarzenboeck[1], Stephan Mertes[7], Franz Martin Schnaiter[3,8], Christiane Voigt[2,9], Mario Mech[10], Susanne Crewell[10], Andreas Herber[11], Christof Lüpkes[11], André Ehrlich[12], Manfred Wendisch[12], and Olivier Jourdan[1]

[1]Laboratoire de Météorologie Physique (LaMP)/OPGC, Université Clermont Auvergne, CNRS/UMR 6016, Clermont-Ferrand, France

[2]Institut für Physik der Atmosphäre, Deutsches Zentrum für Luft- und Raumfahrt, Weßling, Germany

[3]Institute for Atmospheric and Environmental Research, University of Wuppertal, Wuppertal, Germany

[4]Laboratoire de Météorologie Dynamique-IPSL, Sorbonne Université/CNRS/Ecole Normale Supérieure-PSL Université/Ecole Polytechnique-Institut Polytechnique de Paris, Paris, France

[5]Laboratoire Atmosphères, Observations Spatiales (LATMOS)/IPSL, Sorbonne Université, UVSQ, CNRS, Paris, France

[6]Laboratoire d'Optique Atmosphérique (LOA), Université de Lille, CNRS, UMR 8518, Lille, France

[7]Abteilung Atmosphärische Mikrophysik, Leibniz-Institut für Troposphärenforschung, Leipzig, Germany

[8]schnaiTEC GmbH, Wuppertal, Germany

[9]Institut für Physik der Atmosphäre, Johannes Gutenberg-Universität, Mainz, Germany

[10]Institut für Geophysik und Meteorologie, Universität zu Köln, Cologne, Germany

[11]Alfred-Wegener-Institut, Helmholtz-Zentrum für Polar- und Meeresforschung, Bremerhaven, Germany

[12]Leipziger Institut für Meteorologie, Universität Leipzig, Leipzig, Germany

Correspondence: Aymeric Dziduch (Aymeric.Dziduch@uca.fr) and Olivier Jourdan (Olivier.Jourdan@uca.fr)

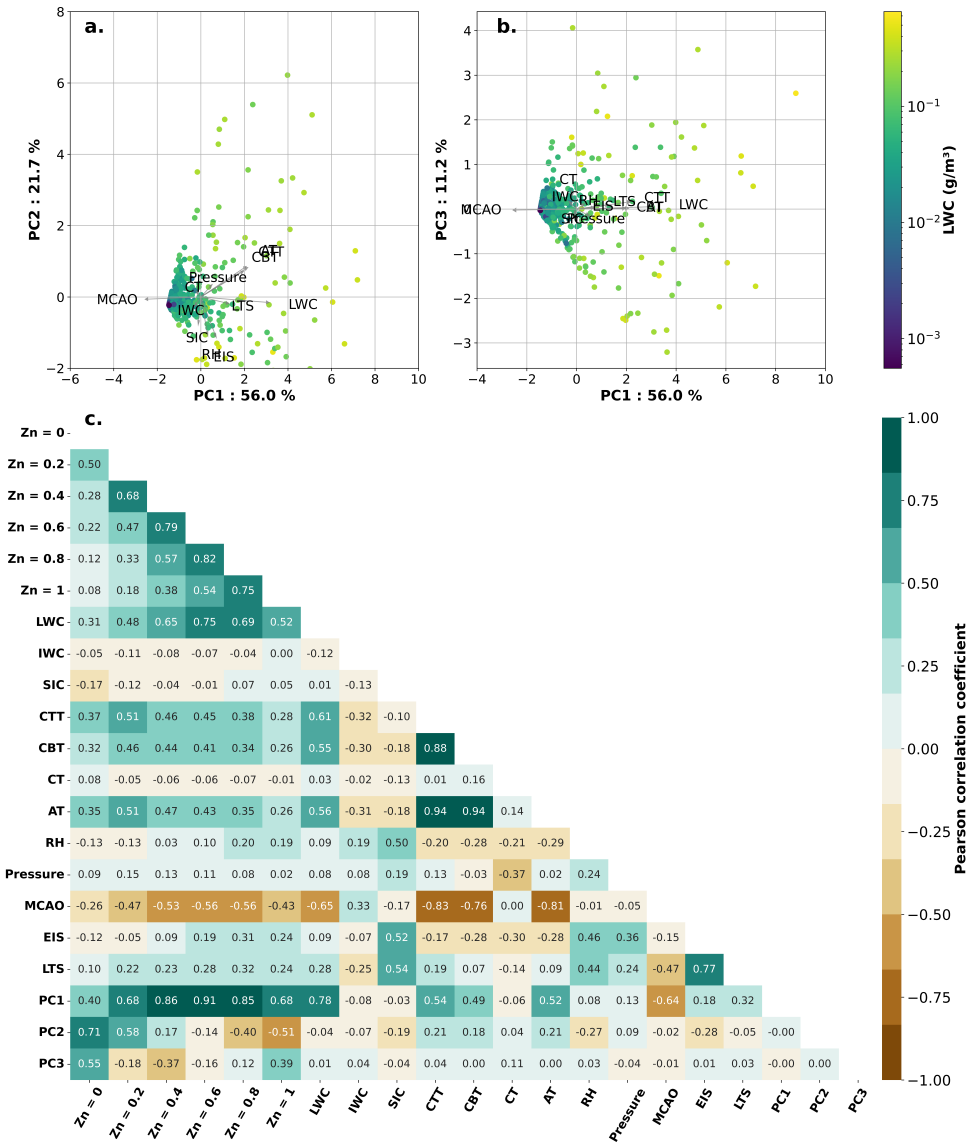

Figure S1. Principal component analysis (PCA) of thermodynamic and microphysical properties for liquid-phase clouds : **(a)** PC1-PC2 and **(b)** PC1–PC3 plane. **(c)** Pearson correlation matrix between the variables and the principal components. Colors indicate the strength and sign of the correlation.

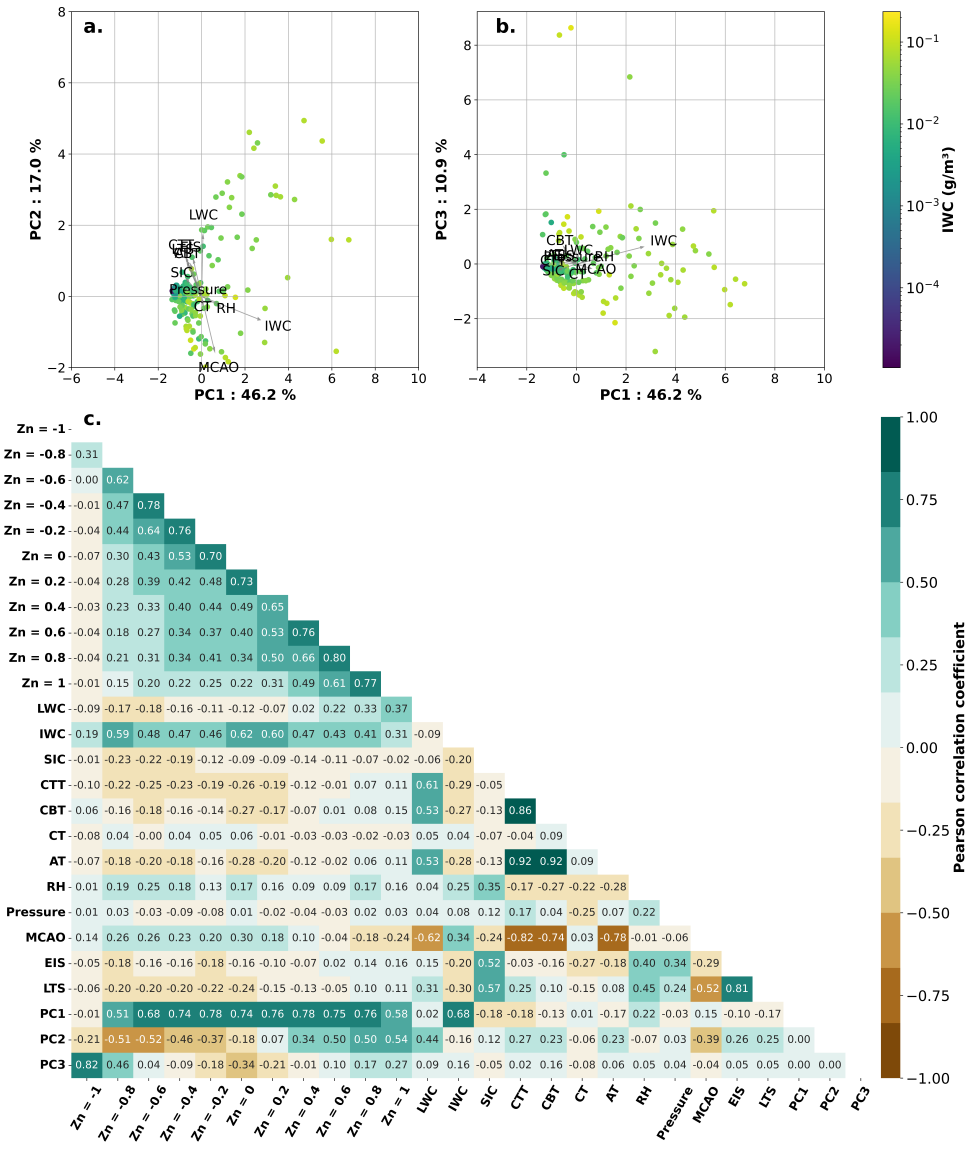

Figure S2. Principal component analysis (PCA) of thermodynamic and microphysical properties for ice-phase clouds : **(a)** PC1-PC2 and **(b)** PC1–PC3 plane. **(c)** Pearson correlation matrix between the variables and the principal components. Colors indicate the strength and sign of the correlation.

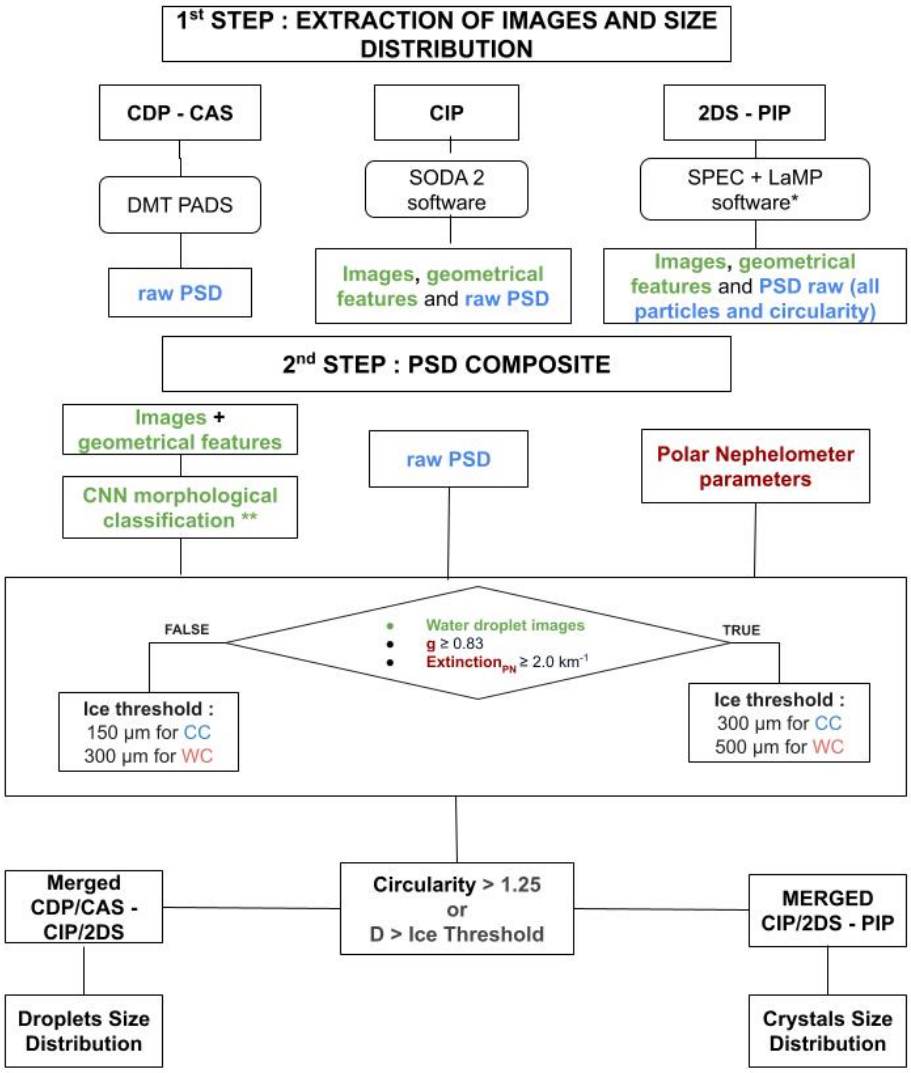

* Leroy et al., (2016)
** Jaffeux et al., (2023)

Figure S3. Description of the data processing and decision tree for the moving threshold

Table S1. Variance explained by the first two principal components (PC1, PC2) for liquid and ice phase clouds, and their correlation with key thermodynamic variables: air temperature (AT), cloud top temperature (CTT), relative humidity (RH), Marine Cold Air Outbreak (MCAO), Estimated Inversion Strength (EIS), and Lower-Tropospheric Stability (LTS).

Principal component	**Variance explained (%)**	**Correlation coefficient**					
		AT	CTT	RH	MCAO	EIS	LTS
Liquid phase							
PC1	56.0	0.52	0.54	0.08	-0.64	0.18	0.32
PC2	21.7	0.21	0.21	-0.27	-0.02	-0.28	-0.05
Ice phase							
PC1	46.2	-0.17	-0.18	0.22	0.15	-0.10	-0.17
PC2	17.0	0.23	0.27	-0.07	-0.39	0.26	0.25

Table S2. Relative error of ice water content (%) with respect to B&L relationship for differents habits and relationship for 2D-S probe. *B&F = Brown and Francis (modified by Hogan to work with Dmax); **Leinonen & Szyrmer with LR for low riming, MR for moderate riming and IR for important riming

Habits	**Heymsfield**	**B&F***	**McFarquhar**	**L&S**- LR**	**L&S - MR**	**L&S - IR**
Co	106	103	32	1	464	1694
CP	−29	−31	−55	−64	95	520
HPC	−33	−31	−53	−70	81	477
CBC	28	21	−25	−32	254	1020
CA	2	−5	−41	−45	182	792
CC	19	18	−22	−43	225	934
FA	55	43	−13	−15	330	1258

Table S3. Macrophysical properties of clouds sampled under different campaigns. Values include the number of sampling legs (N_{leg}), in-cloud measurement time (t_{cld}), and the base (Z_{b}), top (Z_{t}), and thickness (H_{cld}) of the liquid water-containing cloud layer, as well as the cloud-top temperature (T_{top}). Median values are shown with interquartile ranges in brackets.

Campaigns	N_{leg}	t_{cld} (min)	Z_{b} (m)	Z_{t} (m)	H_{cld} (m)	T_{top} (°C)
ACLOUD	56	523	170 [90/220]	520 [410/685]	374 [250/560]	-3.8 [-6.2/-2.2]
AFLUX	74	334	220 [160/360]	510 [380/850]	200 [115/380]	-16 [-17.2/-15]
MOSAiC-ACA	60	308	70 [50/200]	710 [470/1620]	420 [360/840]	-2.6 [-6.3/2.5]
HALO-(AC)^3	78	394	290 [130/430]	650 [620/1000]	450 [340/520]	-15.2 [-17/-11.2]

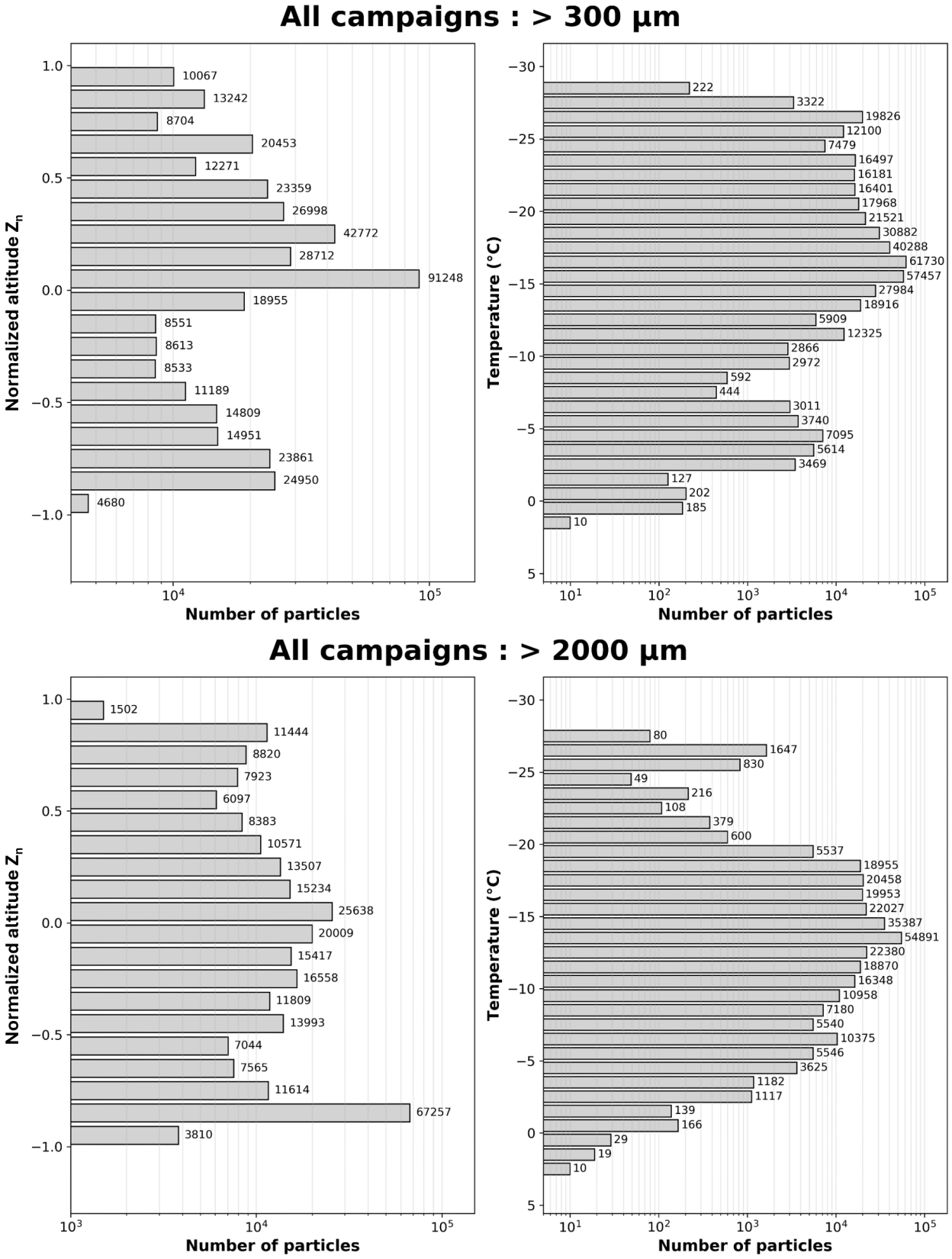

Figure S4. Distribution of the number of classified ice particle images as a function of normalized altitude (Z_n) and temperature for all campaigns, considering particles larger than 300 µm (2D-S and CIP) and 2000 µm (PIP).

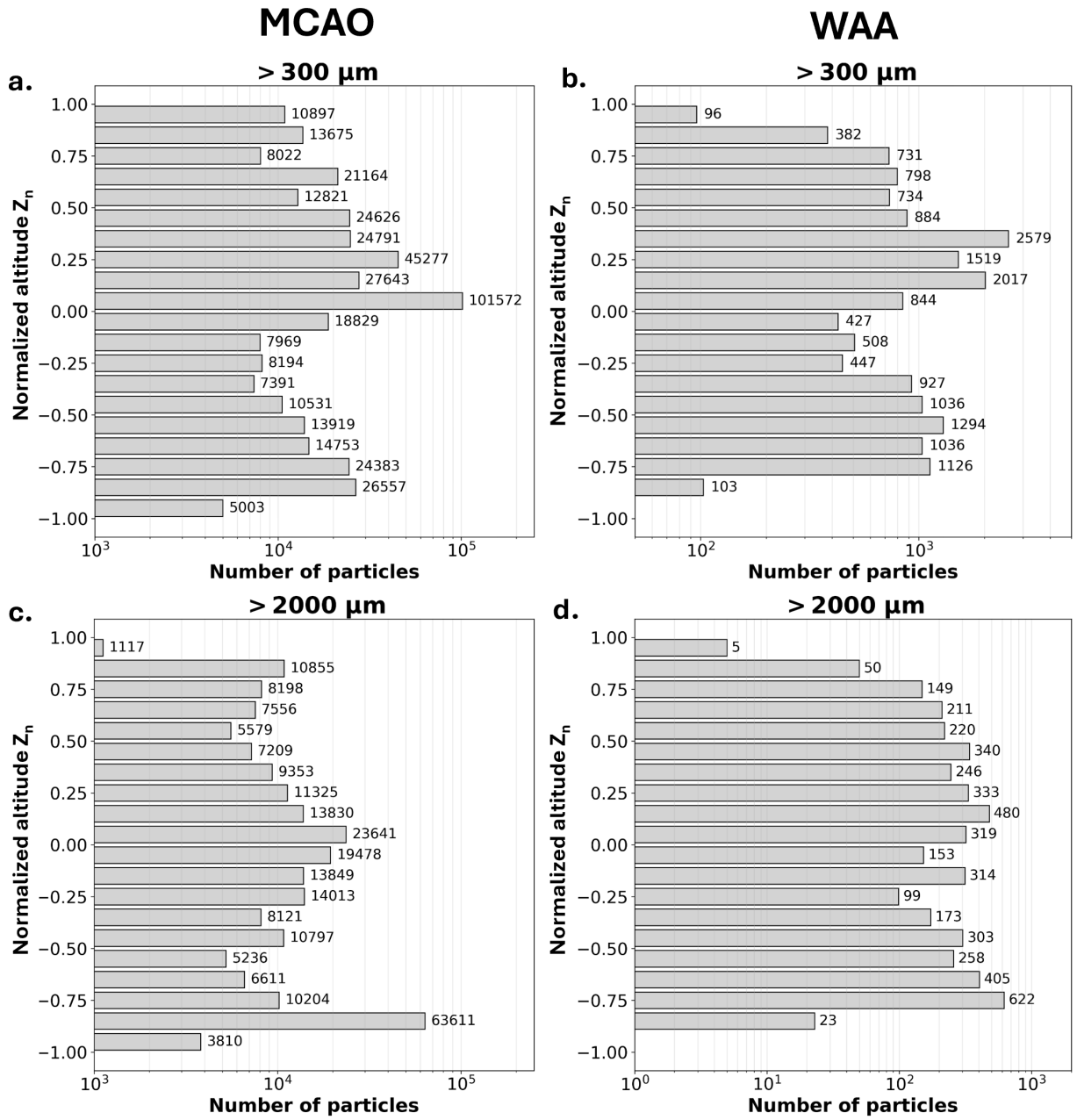

Figure S5. Distribution of the number of classified ice particle images as a function of normalized altitude (Z_n) and temperature for (a-c) MCAO and (b-d) WAA conditions, considering particles larger than 300 µm (2D-S and CIP) and 2000 µm (PIP).

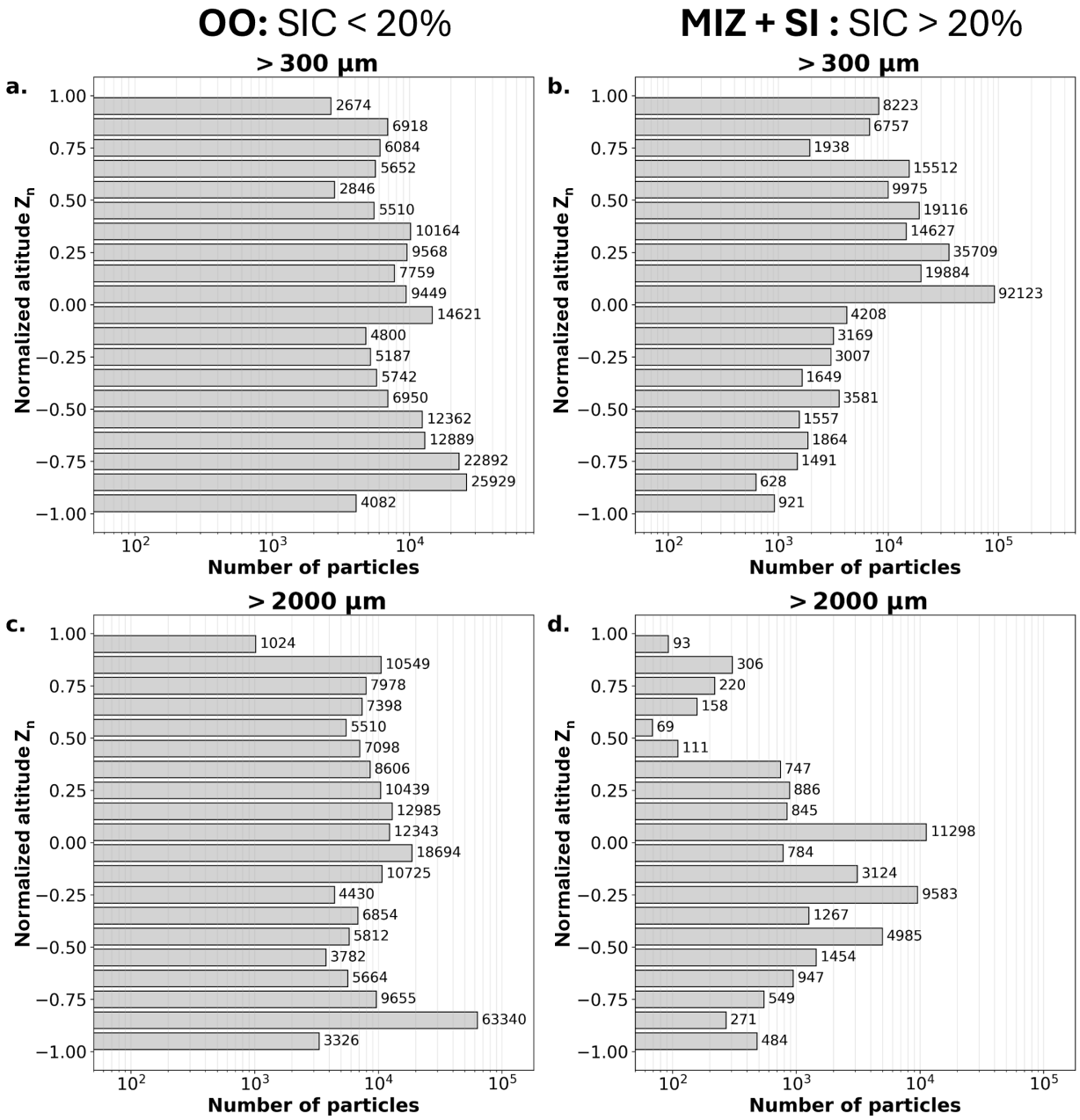

Figure S6. Distribution of the number of classified ice-particle images as a function of normalized altitude (Z_n) and temperature for MCAO conditions over open ocean (OO; sea ice concentration < 20 %) and ice-covered regions (MIZ + SI; sea ice concentration > 20 %), considering particles larger than 300 µm (2D-S and CIP), and particles larger than 2000 µm (PIP).

Text S1.

The influence of environmental parameters on cloud vertical profiles was assessed through a Principal Component Analysis (PCA) performed on the full set of normalized profiles. Each profile was treated as a full vector composed of cloud microphysical property values (IWC and LWC) sampled along the normalized altitude. The PCA was applied to the entire vertical structure of each profile (i.e., the full vector of normalized cloud levels), allowing dimensionality reduction while preserving variance associated with environmental variability. Table S1 summarizes the results of the PCA performed on the normalized vertical profiles for the liquid and ice cloud phases, based on six key environmental parameters: air temperature (AT), cloud top temperature (CTT), relative humidity (RH), marine cold air outbreak index (MCAO), estimated inversion strength (EIS), and lower-tropospheric stability (LTS). The component loads reported in Table S1 are based on the PCA analysis shown in Figures S1 and S2.

For the liquid phase, the first principal component (PC1) explains 56.0 % of the total variance and shows strong positive correlations with AT (0.52) and CTT (0.54), as well as a strong negative correlation with MCAO (–0.64). This component is also most strongly associated with the upper part of the cloud profile and with liquid water content (LWC), as shown in Figure S1, supporting the interpretation that PC1 captures the development of the supercooled liquid layer. PC2 explains 21.7 % of the variance, with weaker correlations overall, but shows moderate negative correlations with EIS and RH (both < –0.25), suggesting a link to moisture and inversion strength in the upper parts of the cloud. These findings are consistent with the role of strong inversions in limiting vertical mixing, thereby concentrating liquid water at the top of the cloud. In contrast, MCAO events enhance turbulence and promote ice nucleation near the cloud base due to cold, dry air entrainment. Overall, these results indicate that the structure and persistence of supercooled liquid cloud layers in Arctic conditions are predominantly controlled by temperature, the origin of the air mass (as indicated by MCAO), and atmospheric stability parameters (EIS and LTS). This highlights the importance of thermodynamic and synoptic controls on liquid-phase clouds.In the ice phase, PC1 accounts for 46.2 % of the total variance but shows only weak correlations with the predictor variables, except for a slight positive correlation with RH (0.22), suggesting that it reflects more general variability not clearly tied to a dominant meteorological control. PC2, which explains 17.0 % of the variance, shows moderate positive correlations with CTT (0.27), EIS (0.26), and LTS (0.25), indicating a connection between atmospheric stability and the vertical structure or depth of the ice cloud layer. Notably, PC2 is more strongly associated with the lower part of the profile and with ice water content (IWC), as shown in Figure S2, and it also exhibits a moderate negative correlation with MCAO (–0.39), reinforcing the idea that marine cold-air outbreaks promote enhanced ice phase.

PCA suggest that MCAO conditions have a strong influence on the structure of mixed-phase clouds. Building on this analysis, we will use the MCAO index as a key environmental parameter to characterize and classify cloud profiles into distinct regimes, enabling a more systematic analysis of mixed-phase cloud variability. In a second step, we will fix the MCAO conditions and explore how variations in atmospheric stability parameters—such as EIS —modulate the vertical structure and phase partitioning of the clouds.

Text S2.

Ice Water Content (IWC) is computed using two distinct relationships: Brown and Francis (1995) modified by Hogan et al. (2012) to use $D_{\max}$ instead of D_{mean}, and Baker and Lawson (2006). The choice of relationship for computing ice water content can lead to significant disparities. To better quantify the impact of this choice on the resulting cloud water content, we compared different mass-diameter relationships using a dataset of 876,908 particles ranging between 300 μm and 3,184 μm. For each individual particle, we extracted geometric features such as maximum diameter, perimeter, area, and width. We then calculated the

mass of each particle according to the mass-diameter relationships reported above (Table S2) and calculated the relative error with respect to the mass of the particles calculated using the Baker & Lawson relationship (Baker and Lawson, 2006) with single combined parameters. We subsequently grouped the results by particle habits classified with the CNN presented above (Jaffeux et al., 2022). As shown in Table S2, different habits exhibit significant discrepancies; most importantly for the present study is the 103% overestimation of column mass from Brown & Francis compared to the Baker & Lawson relationship.

References

Baker, B. and Lawson, R. P.: Improvement in Determination of Ice Water Content from Two-Dimensional Particle Imagery. Part I: Image-to-Mass Relationships, Journal of Applied Meteorology and Climatology, 45, 1282–1290, https://doi.org/10.1175/JAM2398.1, 2006.

Brown, P. R. A. and Francis, P. N.: Improved Measurements of the Ice Water Content in Cirrus Using a Total-Water Probe, J. Atmos. Oceanic Technol., 12, 410–414, https://doi.org/10.1175/1520-0426(1995)012<0410:IMOTIW>2.0.CO;2, 1995.

Hogan, R. J., Tian, L., Brown, P. R. A., Westbrook, C. D., Heymsfield, A. J., and Eastment, J. D.: Radar Scattering from Ice Aggregates Using the Horizontally Aligned Oblate Spheroid Approximation, Journal of Applied Meteorology and Climatology, 51, 655–671, https://doi.org/10.1175/JAMC-D-11-074.1, 2012.

Jaffeux, L., Schwarzenböck, A., Coutris, P., and Duroure, C.: Ice crystal images from optical array probes: classification with convolutional neural networks, Atmos. Meas. Tech., 15, 5141–5157, https://doi.org/10.5194/amt-15-5141-2022, 2022.